



Published in final edited form as:

Science. 2001 August 24; 293(5534): 1499–1503. doi:10.1126/science.1062977.

Crystal Structure of Sensory Rhodopsin II at 2.4 Angstroms: Insights into Color Tuning and Transducer Interaction

Hartmut Luecke^{1,2,*}, Brigitte Schobert², Janos K. Lanyi^{2,*}, Elena N. Spudich³, and John L. Spudich^{3,*}

¹Department of Molecular Biology and Biochemistry, University of California, Irvine, CA 92697, USA

²Department of Physiology and Biophysics, University of California, Irvine, CA 92697, USA

³Department of Microbiology and Molecular Genetics and Structural Biology Center, University of Texas Medical School, Houston, TX 77030, USA

Abstract

We report an atomic-resolution structure for a sensory member of the microbial rhodopsin family, the phototaxis receptor sensory rhodopsin II (NpSRII), which mediates blue-light avoidance by the haloarchaeon *Natronobacterium pharaonis*. The 2.4 angstrom structure reveals features responsible for the 70- to 80-nanometer blue shift of its absorption maximum relative to those of haloarchaeal transport rhodopsins, as well as structural differences due to its sensory, as opposed to transport, function. Multiple factors appear to account for the spectral tuning difference with respect to bacteriorhodopsin: (i) repositioning of the guanidinium group of arginine 72, a residue that interacts with the counterion to the retinylidene protonated Schiff base; (ii) rearrangement of the protein near the retinal ring; and (iii) changes in tilt and slant of the retinal polyene chain. Inspection of the surface topography reveals an exposed polar residue, tyrosine 199, not present in bacteriorhodopsin, in the middle of the membrane bilayer. We propose that this residue interacts with the adjacent helices of the cognate NpSRII transducer NpHtrII.

Microbial rhodopsins are a family of membrane-embedded photoactive retinylidene proteins found throughout the three domains of life: archaea (1–3), eubacteria (4), and unicellular eukaryotes (5, 6). They share a common design of seven transmembrane helices forming an interior pocket for the chromophore retinal, and their functions are driven by a common photochemical reaction—light-induced retinal isomerization—but they carry out two distinctly different functions: light-driven ion transport and photosensory signaling. Both functional types are found in haloarchaea such as *Halobacterium salinarum* and *Natronobacterium pharaonis*. In the haloarchaea, bacteriorhodopsin (BR) and halorhodopsin (HR) are light-driven ion pumps for protons and chloride, respectively (2, 3); and the sensory rhodopsins I and II (SRI and SRII) are phototaxis receptors controlling the cell's swimming behavior in response to changes in light intensity and color (1). The *N. pharaonis* phototaxis receptor NpSRII is 27% identical to BR in amino acid sequence (7) and exhibits

*To whom correspondence should be addressed. hudel@uci.edu (H.L.), jlanyi@orion.oac.uci.edu (J.K.L.), or john.l.spudich@uth.tmc.edu (J.L.S.).

typically ~40% identity with other sensory rhodopsins; all contain ~80% identity in the residues known to form the retinal binding pocket in BR.

Atomic-resolution crystal structures of BR and HR from *H. salinarum* have been obtained by x-ray crystallography (8–10). An intermediate resolution (6.9 Å) projection structure of NpSR_{II} derived from electron crystallography of two-dimensional (2D) crystals showed an overall disposition of the seven helices that was similar to that in the two transport rhodopsins (11). Here we report atomic-resolution information for a microbial sensory rhodopsin, the 2.4 Å structure of NpSR_{II} obtained from x-ray diffraction of 3D crystals grown in a cubic lipid phase.

The overall seven-helical structure is similar to those of the transport rhodopsins BR and HR (8–11). The antiparallel β sheet at the BC loop is two residues shorter than in BR (9). The EF loop participates in crystal packing between bilayer sheets, and helix E is fully ordered with a π-bulge kink (10) at position 154. For data collection and refinement statistics, see Table 1.

Among the known photosensory pigments, a unique property of retinylidene proteins, in microbial rhodopsins as well as higher animal visual pigments, is the tuning of the absorption spectrum of the retinal chromophore over a wide range of the visible region. BR, HR, and SRI in *H. salinarum* absorb green-orange light, with absorption maxima at 570 to 590 nm, whereas SR_{II} exhibits blue-shifted absorption maxima, at 487 and 497 nm for the *H. salinarum* and *N. pharaonis* homologs [HsSR_{II} (12) and NpSR_{II} (13, 14)], respectively. A protonated retinylidene Schiff base compound in methanol/Cl⁻ exhibits maximal absorption at 440 nm (12). Interactions between the retinal chromophore and its protein environment typically shift the absorption to longer wavelengths (the “opsin shift”) (15), resulting in absorption maxima at 497 nm in NpSR_{II} and 568 nm in BR. In the better understood case, BR, three contributing factors have been identified (16): (i) the protein forces the conformation of the C6–C7 single bond in the retinal to be 6s-trans, allowing ring/chain coplanarity; (ii) the positive charge on the protonated Schiff base is only weakly stabilized by a complex counterion provided by the protein environment; and (iii) a less well-defined third factor, which is thought to involve the interaction of polar or polarizable protein groups with the chromophore, destabilizes the ground state or stabilizes the excited state.

The retinal-binding pocket of NpSR_{II} provides insights into structural changes responsible for its blue shift with respect to BR (Figs. 1 and 2). The ring and polyene chain of NpSR_{II} are coplanar as in BR, and therefore we expect a similar opsin shift contribution from this factor. In the case of HsSR_{II}, it has been suggested that ring/chain coplanarity alone is sufficient to explain its relatively small opsin shift to 487 nm (12).

Although one of the important means of modulating the absorption of a protonated retinal Schiff base is to vary its distance to its counterion (15), the two aspartate carboxyls Asp⁷⁵ and Asp²⁰¹ in NpSR_{II} are in nearly identical positions as in BR. Instead, several changes in the structure combine to cause the blue shift from BR by minimizing factors (ii) and (iii), which shift BR absorption to longer wavelengths. The first is a displacement of the guanidinium group of Arg⁷² by 1.1 Å, coupled with a rotation away from the Schiff base in

NpSRII. This increase in distance reduces the influence of Arg⁷² on the counterion, thus strengthening the Schiff base/counterion interaction.

Second, a blue shift is expected (15, 17) from the removal of two hydroxyls near the β -ionone ring from Ser¹⁴¹ and Thr¹⁴² in BR, replaced with nonpolar residues Gly¹³⁰ and Ala¹³¹ in NpSRII. A possible third contributor to the color difference is the change in tilt and slant of the retinal polyene chain, altering the interaction of the conjugated π system with the binding pocket, thereby modulating ground- and excited-state energy levels (Fig. 2A).

Mutagenic substitution of 10 residues, in or near the retinal-binding pocket with their corresponding BR residues, including Gly¹³⁰ to Ser¹⁴¹ and Ala¹³¹ to Thr¹⁴², produced only a ~25-nm red shift of the NpSRII absorption maximum (18, 19). Our interpretation is that these substitutions do not produce the full 71-nm red shift to the BR value, because they do not result in the movements of Arg⁷² and the other retinal pocket residues from their altered positions, which are determined by residue interactions outside the pocket as well as by helix backbone differences between NpSRII and the transport rhodopsins (Fig. 2C). Arg⁷² is repositioned as a consequence of several factors, including movement of its helix backbone by 0.9 Å and the cavity created by changes from BR: Phe²⁰⁸ → Ile¹⁹⁷, Glu¹⁹⁴ → Pro¹⁸³, and Glu²⁰⁴ → Asp¹⁹² (Fig. 2B). Hence the spectral tuning results from precise positioning of retinal binding pocket residues and the guanidinium of Arg⁷², which cannot be deduced from primary structure alone but requires atomic-resolution tertiary structure information.

Wegener *et al.* (20) have used electron paramagnetic resonance spectroscopy to measure the accessibility and static and transient mobility of nitroxide labels placed at the positions of eight residues on the cytoplasmic side of helices F and G in NpSRII. They concluded that Lys¹⁵⁷ and Ser¹⁵⁸ are oriented toward the aqueous phase; Leu¹⁵⁹, Tyr¹⁶⁰, Ile²¹¹, and Leu²¹³ face the protein interior; and Phe²¹⁰ and Ala²¹² are located at the protein/lipid bilayer interface. Each of these assignments is confirmed by the crystal structure except Ile²¹¹, which is on the surface of helix G facing the hydrophobic portion of the bilayer. A possible explanation of the contrasting assignment of Ile²¹¹ is that the spin-label nitroxide distorts the structure. Further, light-induced changes in the spin labels indicated movement of helix F with negligible movement of helix G (20). The disconnection of the two helices was suggested as possibly being due to the predicted absence of the π bulge in helix G (20), but we observe the π bulge to be present in the NpSRII structure, indicating that the apparent dissociation of helices F and G in the spin-labeling study must be attributable to other factors.

The sensory rhodopsins do not pump ions when complexed with their cognate transducers, but in some cases light-driven vectorial translocation of protons does occur in the absence of transducer (21). Substantial proton transport by NpSRII required factors that are expected to increase cytoplasmic-side proton conductivity (the presence of sodium azide and the Phe⁸⁶ → Asp⁸⁶ mutation), and both wild-type NpSRII and HsSRII circulate protons primarily to and from the extracellular side. In the structure, the low proton conductivity on the cytoplasmic side is evident in that the Asp⁹⁶-Thr⁴⁶ pair in the cytoplasmic channel of BR is replaced by the Phe⁸⁶-Leu⁴⁰ pair and presents a hydrophobic barrier (22). The greater

hydrophobicity of the cytoplasmic side is attested by the presence of a detergent molecule (β -octylglucoside) that is inserted with its C8 tail perpendicular to the bilayer into the middle of the seven-helix bundle, almost reaching the side chain of Phe⁸⁶.

A fundamental question is how the common design of microbial rhodopsin proteins has been adapted to carry out their two distinct functions. Transport rhodopsins function independently of interaction with other proteins and translocate ions through an intramolecular channel. Sensory rhodopsins, on the other hand, transmit signals by protein-protein interaction with transducer proteins that control cytoplasmic enzymatic activity (7, 23, 24). In HsSRI and HsSR II, the receptors form a molecular complex with their cognate integral membrane transducer proteins, HtrI and HtrII, respectively, which in turn modulate a cytoplasmic phosphorylation pathway that controls the cell's motility apparatus (1). Chimera experiments with the *H. salinarum* transducers showed that the interaction specificities of SRI with HtrI and SR II with HtrII are determined by the transmembrane helices of the Htr subunits (25), indicating that interaction occurs within or near the membrane. A fragment of NpHtrII lacking most of the cytoplasmic domain interacts with NpSR II in vitro, supporting the idea that transmembrane helix-helix interactions occur also in the *N. pharaonis* pair (20). Bearing on the possible location of the transducer-binding surface of the receptor, the structure of NpSR II reveals that a tyrosine residue protrudes from the lipid-facing surface of helix G (Fig. 3). Unlike threonine or serine hydroxyls, which can hydrogen-bond to main-chain carbonyls of their own helix, the tyrosine phenol group is too long and rigid to allow the formation of such hydrogen bonds. To avoid an unpaired polar hydroxyl in the middle of the bilayer, in the 3D crystals, and presumably in the 2D crystals as well, the Tyr¹⁹⁹ hydroxyl forms an intermolecular hydrogen bond to the main-chain carbonyl of a transmembrane helix from a neighboring molecule in the same bilayer (Ala¹²⁵ in helix E). Tyr¹⁹⁹ is conserved in the three known SR II sequences, whereas this residue is a phenylalanine in the two known SRI sequences (1). The need to hydrogen-bond to an adjacent protein makes Tyr¹⁹⁹ an excellent candidate for transducer binding in the SR II-HtrII complex in *N. pharaonis* membranes. The hydrophobic surface of NpSR II displays three distinct faces: face I is defined by helices F, G, and A; face II by helices A (the CP half), B, C, D, and E (the EC half); and face III by helices E and F. Tyr¹⁹⁹ is located prominently in the middle of face I, the face that also contains both helices known to undergo large motions during the BR photocycle (26). It is thus likely that face I provides the majority of the interaction with the photosignal transducer. Other residues on the outside of helix G also show clear grouping between the SRI and SR II subfamilies, possibly contributing to transducer binding specificity.

Acknowledgments

We thank R. R. Birge for discussions regarding spectral tuning in NpSR II and BR, C. Riekel for access to the microfocus beamline at the European Synchrotron Radiation Facility (ESRF), and J.-P. Cartailleur for assistance with Fig. 2C. Supported by NIH grants R01-GM59970 (H.L.), R01-GM29498 (J.K.L.), and R01-GM27750 (J.L.S.); Department of Energy grant DEFG03-86ER13525 (J.K.L.); and a Robert A. Welch Foundation award (J.L.S.). The atomic coordinates of NpSR II have been deposited in the Protein Data Bank (PDB) with the entry name of 1JGJ.

References and Notes

1. Hoff WD, Jung KH, Spudich JL. *Annu Rev Biophys Biomolec Struct.* 1997; 26:223.

2. Oesterhelt D. *Curr Opin Struct Biol.* 1998; 8:489. [PubMed: 9729742]
3. Lanyi JK. *J Phys Chem.* 2000; 104:11441.
4. Béjà O, et al. *Science.* 2000; 289:1902. [PubMed: 10988064]
5. Bieszke JA, Spudich EN, Scott KL, Borkovich KA, Spudich JL. *Biochemistry.* 1999; 38:14138. [PubMed: 10571987]
6. Spudich JL, Yang CH, Jung KH, Spudich EN. *Annu Rev Cell Dev Biol.* 2000; 16:365. [PubMed: 11031241]
7. Seidel R, et al. *Proc Natl Acad Sci USA.* 1995; 92:3036. [PubMed: 7708770]
8. Belrhali H, et al. *Structure.* 1999; 7:909. [PubMed: 10467143]
9. Luecke H, Schobert B, Richter HT, Cartailler JP, Lanyi JK. *J Mol Biol.* 1999; 291:899. [PubMed: 10452895]
10. Kolbe M, Besir H, Essen LO, Oesterhelt D. *Science.* 2000; 288:1390. [PubMed: 10827943]
11. Kunji ERS, Spudich EN, Grisshammer R, Henderson R, Spudich JL. *J Mol Biol.* 2001; 308:279. [PubMed: 11327767]
12. Takahashi T, et al. *Biochemistry.* 1990; 29:8467. [PubMed: 2252905]
13. Hirayama J, et al. *Biochemistry.* 1992; 31:2093. [PubMed: 1536851]
14. Chizov I, et al. *Biophys J.* 1998; 75:999. [PubMed: 9675200]
15. Nakanishi K, et al. *Photochem Photobiol.* 1979; 29:657. [PubMed: 451005]
16. Yan B, et al. *J Biol Chem.* 1995; 270:29668. [PubMed: 8530353]
17. Spudich JL, et al. *Biophys J.* 1986; 49:479. [PubMed: 2937462]
18. Shimono K, Iwamoto M, Sumi M, Kamo N. *Photochem Photobiol.* 2000; 72:141. [PubMed: 10911739]
19. Kamo N, Shimono K, Iwamoto M, Sudo Y. *Biochemistry (Moscow).* in press.
20. Wegener AA, Chizhov I, Engelhard M, Steinhoff HJ. *J Mol Biol.* 2000; 301:881. [PubMed: 10966793]
21. HtrI-free HsSRI was shown to exhibit single photon-induced proton pumping out of cell envelope vesicles at pH > 7 [Bogomolni RA, et al. *Proc Natl Acad Sci USA.* 1994; 91:10188. [PubMed: 7937859]]. In cell envelope vesicles, HsSR II exhibits only electroneutral light-induced circulation of protons to and from the extracellular medium [Sasaki J, Spudich JL. *Biophys J.* 1999; 77:2145. [PubMed: 10512834] NpSR II was found to have some proton transport activity in such vesicles [Sudo Y, Iwamoto M, Shimono K, Sumi M, Kamo N. *Biophys J.* 2001; 80:916. [PubMed: 11159458] as well as in black lipid films [Schmies G, et al. *Biophys J.* 2000; 78:959. [PubMed: 10653808]]. When expressed in *Xenopus* oocytes, HsSR II exhibited weak proton transport and NpSR II did not show any stationary photocurrent [Schmies G, Engelhard M, Wood PG, Nagel G, Bamberg E. *Proc Natl Acad Sci USA.* 2001; 98:1555. [PubMed: 11171989]
22. The cytoplasmic region of NpSR II lacks a nucleation site for the development of a hydrogen-bonded network of water molecules [Luecke H, et al. *J Mol Biol.* 2000; 300:1237. [PubMed: 10903866] Also, the extracellular region lacks proton release machinery; that is, a pair of glutamic acid residues connected to the Schiff base region by a 3D hydrogen-bonded network of side chains and water (9) [Rammelsberg R, Huhn G, Lübben M, Gerwert K. *Biochemistry.* 1998; 37:5001. [PubMed: 9538019] that prevents the return of the proton from the extracellular side in bacteriorhodopsin [Balashov SP, Imasheva ES, Govindjee R, Ebrey TG. *Biophys J.* 1996; 70:473. [PubMed: 8770224] Richter H-T, Brown LS, Needleman R, Lanyi JK. *Biochemistry.* 1996; 35:4054. [PubMed: 8672439] A similar situation arises in the Asp96 → Asn96 mutant of BR at a pH below the pK for proton release; but unlike NpSR II, this protein exhibits transport. In BR, although at pH < 6 protonation equilibrium between the Schiff base and its counterion ensures that the proton can pass to the extracellular side [Brown LS, Dioumaev AK, Needleman R, Lanyi JK. *Biophys J.* 1998; 75:1455. [PubMed: 9726947] at the low pH the reprotonation from the cytoplasmic side is strongly accelerated [Miller A, Oesterhelt D. *Biochem Biophys Acta.* 1990; 1020:57. In contrast, the cytoplasmic region of NpSR II is likely to be a permanent barrier to protons. If directionality is conferred on the movement of the transported ion by the changing ion conductivities of the extracellular and cytoplasmic regions [Brown LS, Dioumaev AK, Needleman R, Lanyi JK. *Biochemistry.* 1998; 37:3982. reprotonation of the Schiff base in NpSR II will be, of necessity, from the extracellular rather than the cytoplasmic side. [PubMed: 9521720]

23. Yao VJ, Spudich JL. Proc Natl Acad Sci USA. 1992; 89:11915. [PubMed: 1465418]
24. Zhang W, Brooun A, Mueller MM, Alam M. Proc Natl Acad Sci USA. 1996; 93:8230. [PubMed: 8710852]
25. Zhang XN, Zhu J, Spudich JL. Proc Natl Acad Sci USA. 1999; 96:19722.
26. Subramaniam S, Henderson R. Nature. 2000; 406:653. [PubMed: 10949309]
27. Landau EM, Rosenbusch JP. Proc Natl Acad Sci USA. 1996; 93:14532. [PubMed: 8962086]
28. Otwinowski, Z. Data Collection and Processing. Sawyer, L.; Isaacs, N.; Bailey, S., editors. SERC Daresbury Laboratory; Warrington, UK: 1993. p. 56-62.
29. Brunger, AT. X-PLOR, Version 3.1: A System for X-Ray Crystallography and NMR. Yale Univ. Press; New Haven, CT: 1992.
30. Brunger AT, et al. Acta Crystallogr D. 1998; 54:905. [PubMed: 9757107]
31. Sack JS. J Mol Graphics. 1988; 6:224.
32. Luecke H, Richter HT, Lanyi JK. Science. 1998; 280:1934. [PubMed: 9632391]
33. Guex N, Peitsch MC. Electrophoresis. 1997; 18:2714. [PubMed: 9504803]

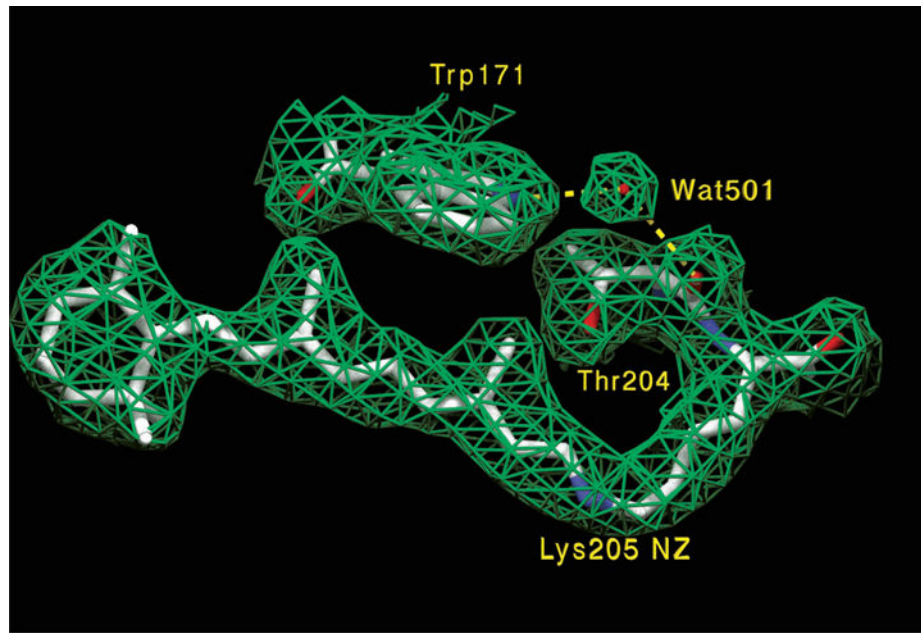


Fig. 1. Electron density map ($2|F_o| - |F_c|$, contoured at 1σ) and corresponding molecular model of the retinal binding pocket. As in BR and HR, the all-trans retinal polyene chain is coplanar with the beta-ionone ring, which is in the 6s-trans conformation. Wat⁵⁰¹ is bridging helices F (Trp¹⁷¹) and G (Thr²⁰⁴ carbonyl). In addition, Wat⁵⁰¹ is also hydrogen-bonding with Thr¹⁶⁷ OH (not shown).

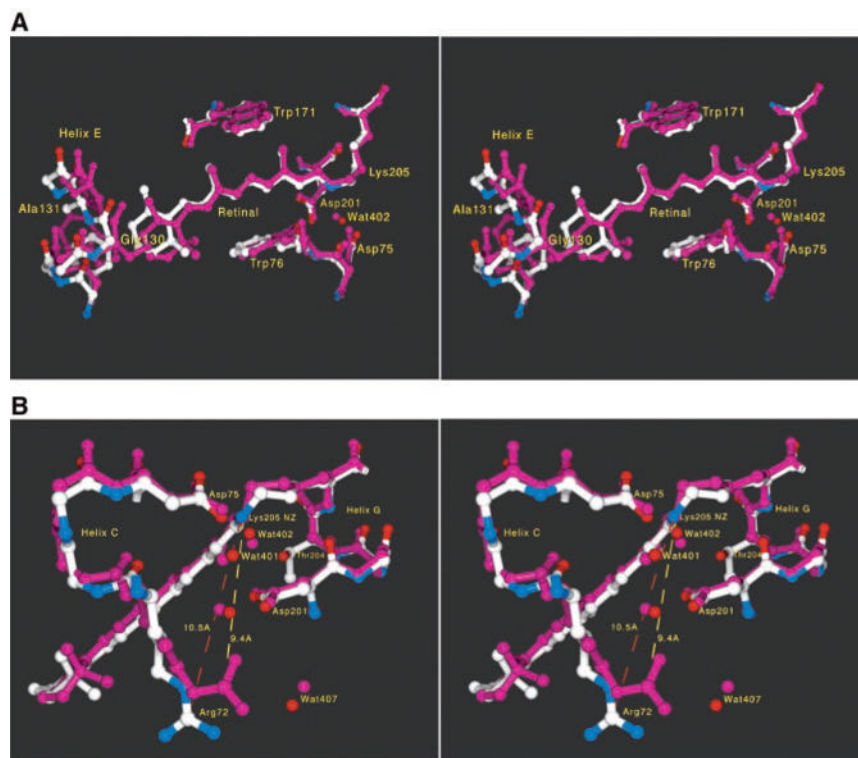


Fig. 2. Comparison of NpSR II and BR structures. The coordinates were aligned with the Iterative Magic Fit procedure of Swiss-PDBViewer version 3.7b2 (33), yielding a root mean square deviation of 0.96 Å for 816 main-chain atoms (BR is shown in purple; NpSR II is shown in white, blue, and red). **(A)** Stereo view of the retinal binding pocket. There is a change in the tilt of the whole polyene chain, presumably largely due to extra room near the end of the ring (C3 and C4 atoms) because of a combination of smaller side chains on residues 130/131 (Gly¹³⁰/Ala¹³¹ in NpSR II, Ser¹⁴¹/Thr¹⁴² in BR) and a local outward bowing of the backbone of helices E and F by up to 1.3 Å [see (C)]. The Ser¹⁴¹/Thr¹⁴² pair in BR, not labeled in the figure, contributes two hydroxyl groups, which are evident as purple protruding from helix E toward the ring. And despite equivalent retinal stereochemical restraints in refinement, the distance from the Schiff base nitrogen (NZ) to retinal C4 increases from 14.0 to 14.6 Å, resulting in a more linear (or less bent) polyene chain in NpSR II. The relative positions of the protonated Schiff base nitrogen and the two negatively charged aspartate carboxylates of Asp⁷⁵ and Asp²⁰¹ are nearly unchanged. However, the electron density for the water molecule found between the Schiff base and these two carboxylates (Wat⁴⁰²) (9, 32) is very weak, suggesting that this water is either more mobile or not fully occupied in NpSR II. In contrast, waters 401, 406, and 501 are well ordered (9). The π bulge of helix G at residue 204 is also present as it is in BR (9) and HR (10), despite the bulkier side chain (Thr²⁰⁴) at this position. **(B)** Stereo view of the Schiff base and the complex counterion. The guanidinium of Arg⁷² moves 1.1 Å away (10.5 versus 9.4 Å) from the Schiff base nitrogen and also reorients its Ne hydrogen. This movement becomes possible because several side chains in the region between Arg⁷² and the extracellular side (below Arg⁷² in the figure) have reduced volumes (Phe²⁰⁸ → Ile¹⁹⁷, Glu¹⁹⁴ → Pro¹⁸³, and

Glu²⁰⁴ → Asp¹⁹²). (C) Plot of distance versus residue number. The average main-chain distance between NpSR_{II} and BR is plotted as a function of residue number (BR numbering). The largest deviations are at the shortened antiparallel β sheet in the BC loop (near residue 70) and at the COOH-terminus, which is being displaced by a detergent molecule.

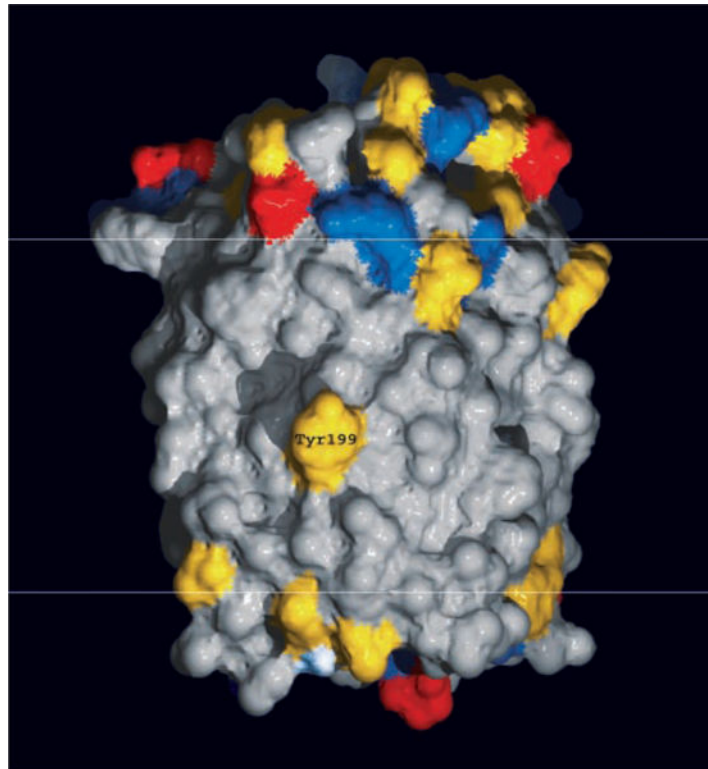


Fig. 3.

Exposed conserved tyrosine in middle of the bilayer. The NpSR II surface (CP side, top; EC side, bottom) is colored according to amino acid type (red, negatively charged; blue, positively charged; yellow, polar; gray, hydrophobic). Residue Tyr¹⁹⁹ is situated in the middle of the bilayer (whose hydrophobic portion lies between the white horizontal lines) near a π bulge on the outside of helix G one-and-a-half helix turns from the lysine (Lys²⁰⁵) to which the retinal is attached.

Table 1

X-ray data collection, molecular replacement, and refinement statistics. Crystals were grown from a cubic lipid phase (27) using octylglucoside-purified NpSRII (28.0 mg/ml) preincubated with *H. salinarum* polar lipids (11.2 mg/ml) (11). Ten-microliter aliquots were mixed with 10 μ l of monoolein glyceride (Nu-Check Prep., MI) and centrifuged for 1 hour at 11,000*g* at 22°C. After overnight incubation at 22°C, precipitant was added. The crystals used were thin rods about 5 μ m by 20 μ m by 200 μ m and were examined 5 weeks after the addition of 50 μ l of 3.5 M KCl in 50 mM MES (pH 5.3) as precipitant. Addition of exogenous *H. salinarum* polar lipids was essential for crystal formation. The crystals belong to space group $C222_1$, with $a = 87.34$ Å, $b = 130.81$ Å, and $c = 50.87$ Å, and consist of bilayers stacked in the b direction. The a and c cell dimensions, as well as the packing, are very similar to those reported for 2D crystals of NpSRII (11). Diffraction data were collected on one cryocooled crystal at the microfocus beamline ID13 at ESRF (Grenoble), using a MAR Research charge-coupled device detector. Each image was 1° in ϕ , with an exposure time of 2 s. Images were reduced, scaled, and merged with the programs DENZO/SCALEPACK (28). Molecular replacement was carried out with the program X-PLOR (29), using the coordinates of the 1.55 Å bacteriorhodopsin structure (PDB code 1C3W, protein without retinal) and yielded an initial R factor of 49.2% (4 to 12 Å). Successive rounds of refinement and model building with the programs CNS (30) and CHAIN (31) using annealed simulated omit and $3|F_o| - 2|F_c|$ maps resulted in an R factor of 23.3%, and an R_{free} of 28.0% for all data between 2.4 and 20 Å without σ cutoff. In many regions near the hydrophobic protein surface, long tubes of density are present for native dihydrophytyl lipids, which as in the case of BR remained tightly bound to the protein through solubilization and cubic lipid phase crystallization. All peptide bonds fall into the allowed regions of the Ramachandran plot.

<i>Data reduction resolution range</i>	<i>2.4–20.0 Å</i>	<i>2.40–2.44 Å</i>
Total observations	80,761	
Unique structure factors	10,704	520
R_{merge} (%)	9.5	44.0
Average $I/\sigma(I)$	5.7	1.3
Completeness (%)	92.2	92.0
Mosaicity (°)	0.86	
<i>Refinement resolution range</i>	<i>2.4–20.0 Å</i>	
R factor (%) for working set, no σ cutoff	23.3	
R_{free} (%) for 8.7% of the unique structure factors	28.0	
Deviation from ideal bond lengths (Å)	0.0086	
Deviation from ideal bond angles (°)	1.29	